American Mineralogist, Volume 74, pages 549–564, 1989

Transmission electron microscopy of chloritoid: Intergrowth with sheet silicates and reactions in metapelites

Jillian F. Banfield
Department of Earth and Planetary Sciences, The Johns Hopkins University, Baltimore, Maryland 21218, U.S.A.
Paul Karabinos
Department of Geology, Williams College, Williamstown, Massachusetts 01267, U.S.A.
David R. Veblen
Department of Earth and Planetary Sciences, The Johns Hopkins University, Baltimore, Maryland 21218, U.S.A.

Abstract

Chloritoid specimens with contrasting metamorphic histories have been studied with high-resolution and analytical transmission electron microscopy. The observations show that chloritoid, an orthosilicate, can intergrow coherently with several sheet silicates and that a wide variation in microstructures can result from different metamorphic histories.

Chloritoid crystals in garnet- and staurolite-grade, aluminous metapelites from the Green Mountains massif near Jamaica, Vermont, experienced a complex polymetamorphic history including both prograde and strong retrograde events. They contain narrow lamellae of chlorite (generally 8.5 to 20 nm wide), stilpnomelane (generally 3.6 to 14.4 nm wide), as well as larger chlorite, paragonite, and berthierine lamellae (80 to 400 nm wide). The intergrown minerals exhibit stacking disorder and mixed layering. In many cases, almost perfect intergrowth on (001) is observed, with structural continuity across many of the grain boundaries. In such intergrowths, b of chloritoid ($C2/c$) is parallel to a of chlorite ($C2/m$) and b of stilpnomelane. All of the minerals can intergrow readily on (001) because of the dimensional similarity between the unpolymerized tetrahedral layer of chloritoid and the tetrahedral sheets of the other minerals. Although the intergrowth textures do not provide conclusive evidence, it is suggested that these coexisting layer structures formed by retrograde replacement of the chloritoid, rather than by parallel growth or prograde reaction of chlorite to form chloritoid. The nucleation of arrays of very narrow chlorite lamellae throughout the chloritoid may have resulted from supersaturation with respect to Mg during retrograde metamorphism.

In contrast to the higher-grade Green Mountains samples, chloritoids from the Taconic Range, Vermont, grew at the peak of a single prograde metamorphic event and are texturally simple, with no intergrown sheet silicates. Although much of the chloritoid nucleated and grew in a muscovite, paragonite, and chlorite matrix, it did not replace the sheet silicates by direct topotactic reaction. The reaction that defines the chloritoid isograd in the Taconic Range occurs by a dissolution and reprecipitation mechanism.

Introduction

Although seldom abundant, chloritoid is an important index mineral in aluminous, Fe-rich metamorphic rocks, its first appearance in some cases being mapped as an isograd. The structure of chloritoid consists of two distinct types of octahedral sheets that are bonded together by layers of isolated silicate tetrahedra. Thus, it is an orthosilicate (island silicate), but the octahedral sheets are similar to those of sheet silicates. As a result, chloritoid exhibits physical properties commonly associated with the latter group, such as perfect cleavage, and structural properties such as ordered polytypes (Halferdahl, 1961) and stacking disorder (Jefferson and Thomas, 1978). The crystal chemistry of chloritoid has been reviewed in detail by Ribbe (1982).

Although their structures are related, the intergrowth of chloritoid with sheet silicates in crystallographically controlled orientations has been reported only recently (Karabinos, 1981) and has been examined only with standard petrographic and analytical techniques. In the present work, we have used high-resolution transmission electron microscopy (HRTEM), X-ray analytical electron microscopy (AEM), and selected-area electron diffraction (SAED) to study chloritoid from two different regions in Vermont having contrasting metamorphic histories. These observations clarify the crystal-chemical principles involved in the fine-scale intergrowth of chloritoid with other minerals. In addition, they shed some light on the mechanisms of reactions involving chloritoid, including the isograd-defining reaction that results in the first ap-

0003–004X/89/0506–0549$02.00

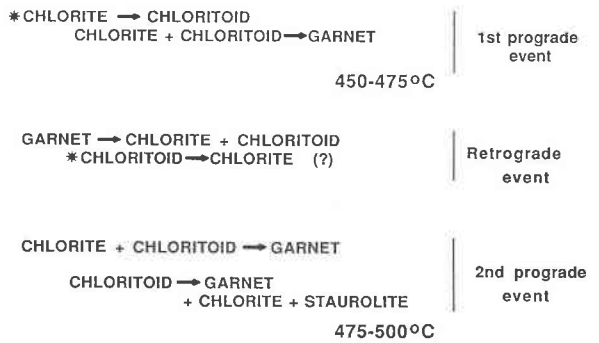

Fig. 1. Simplified compilation of the mineral reactions and peak metamorphic temperatures determined for the Hoosac Formation schists, Jamaica, Vermont (Karabinos, 1981). Asterisks indicate reactions discussed in the text.

pearance of chloritoid during prograde metamorphism of aluminous, Fe-rich pelitic rocks.

Observations using HRTEM have repeatedly demonstrated that mineral intergrowths recognized in the petrographic microscope can occur on a very fine scale, down to the unit-cell level. In addition, such observations, combined with other geologic information, commonly can be used to infer the processes that result in such intergrowths. In sheet silicates, intergrowths can arise from exsolution (Veblen, 1983a) or primary growth processes (Iijima and Zhu, 1982). However, the fine-scale interlayering of sheet silicates most commonly has been attributed to replacement reactions that may result from retrograde metamorphism, hydrothermal alteration, weathering, diagenesis, or other processes (e.g., Veblen and Ferry, 1983; Banfield and Eggleton, 1988; Ahn and Peacor, 1986).

Specimen description and experimental methods

Samples of chloritoid-bearing rocks used in this study are from two areas with contrasting geologic histories. The first set of samples (specimen numbers 625, 333, and 561 of Karabinos, 1981) is representative of Hoosac Formation schists from the east side of the Green Mountains massif near Jamaica, Vermont, which have been subjected to multiple episodes of deformation and regional metamorphism (Fig. 1). During an early episode of deformation, these rocks reached the garnet grade of metamorphism. This prograde event was followed by widespread and intense retrogression, which led to partial resorption of garnet and produced some retrograde chlorite (Karabinos, 1981, 1984). A later deformation was accompanied by a second stage of garnet growth, which resulted in textural unconformities described by Rosenfeld (1968) and Karabinos (1984). These textures were illustrated by Karabinos (1984, Fig. 9). Some of the Jamaica rocks reached staurolite grade during this second prograde event. Medium-pressure facies-series conditions have been estimated for these rocks (Karabinos and Laird, 1988). Temperature estimates based on the mineral assemblages and results of Spear and Cheney (1989), are included in Figure 1.

The Green Mountains schists we have investigated contain chloritoid and chlorite, coarse-grained muscovite, fine-grained paragonite, quartz, centimeter-sized garnet, epidote, apatite, rutile, and tourmaline; staurolite is present in some higher-grade samples (Karabinos, 1981). The chloritoid crystals are subhedral and generally between 0.2 and 0.3 mm in longest dimension. Typically, both chloritoid and chlorite grains are elongate and parallel to the dominant foliation, although some randomly oriented grains of retrograde chlorite also are present.

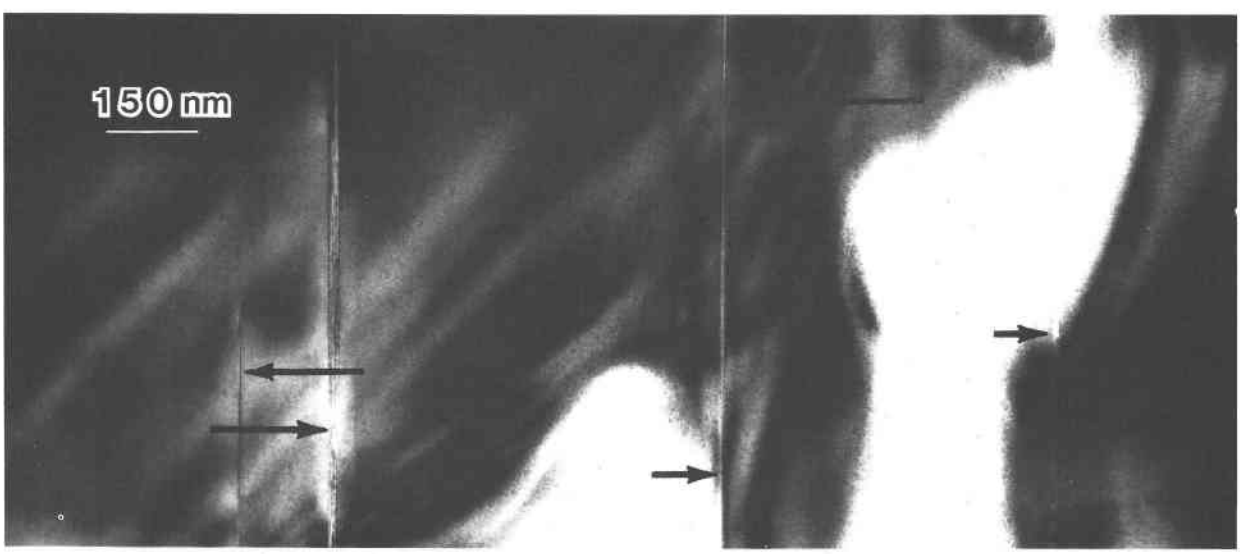

Fig. 2. Bright-field transmission electron micrograph of narrow chlorite lamellae (indicated by arrows) in chloritoid from Jamaica, Vermont.

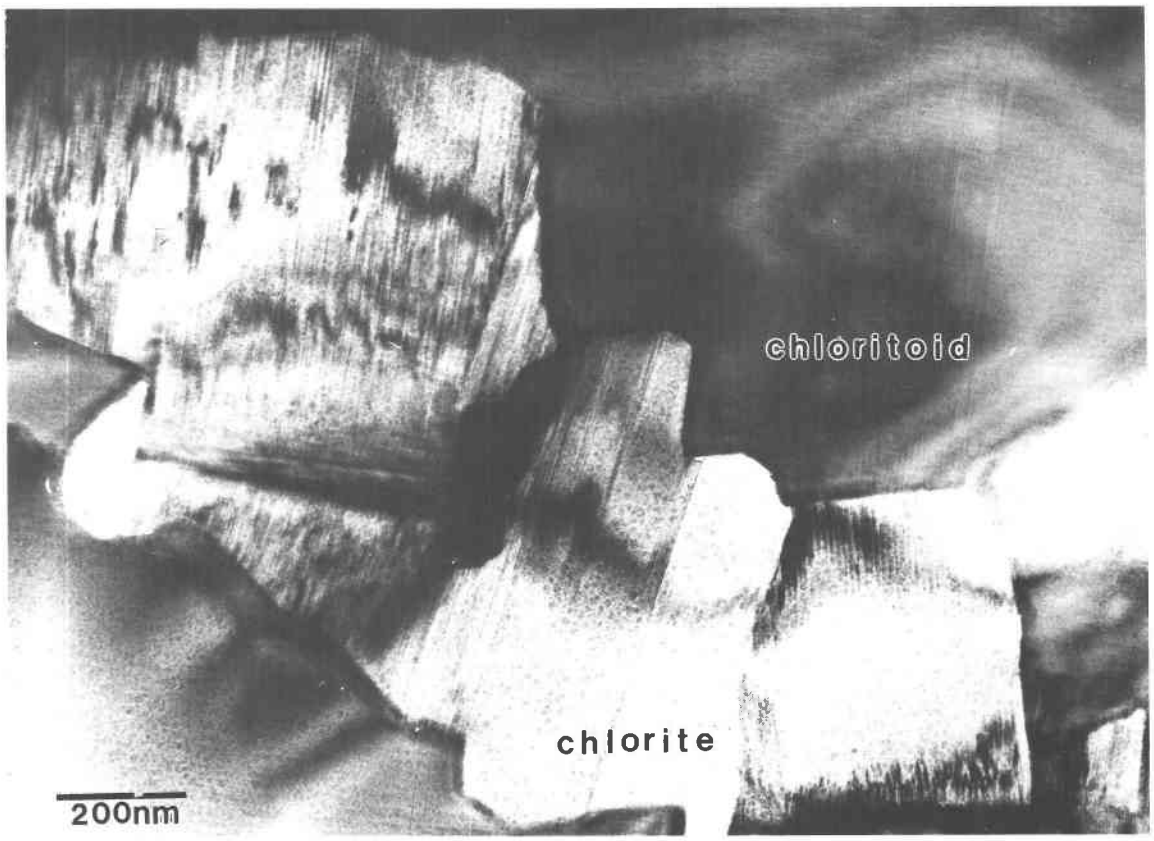

Fig. 3. Large chlorite crystals with variable orientations in a channel in chloritoid.

Karabinos (1981) has shown that during each simultaneous prograde metamorphic and deformational event, these rocks remained approximately in chemical and textural equilibrium. The intermediate episode of retrograde metamorphic mineral growth occurred under static metamorphic conditions.

Samples 2112 and 2113 were collected along Vermont Route 4 west of Rutland, very close to the chloritoid isograd in the Taconic Range, as mapped by Zen (1960, 1967). These low-grade metapelites are thus interpreted to represent the first growth of chloritoid resulting from a single, prograde regional metamorphic event. As described previously by Zen (1960), these fine-grained phyllites contain muscovite, paragonite, quartz, chlorite, chloritoid, rutile, and hematite. In thin section, chloritoid crystals up to approximately 20 μm long can be observed, but TEM study shows that most chloritoid crystals in these rocks are smaller than 1 μm.

Thin foils were prepared for electron microscopy by ion milling 2.3-mm discs removed from petrographic thin sections. Specimens were lightly coated with C and examined in a Philips 420T transmission electron microscope operated at 120 keV. Images were obtained from thin areas at a range of underfocus values around -80 nm. Interpretation of HRTEM images from the sheet silicates follows that of previous papers (e.g., Spinnler et al., 1984; Veblen, 1983a, 1983b; Eggleton and Banfield, 1985; Jefferson and Thomas, 1978; Iijima and Buseck, 1978; Amouric et al., 1981). Because image simulations for chloritoid have not been published previously, we performed calculations of images as a function of crystal thickness and microscope defocus in order to interpret our chloritoid images correctly. The results from these simulations are outlined in Appendix 1. The identity of minerals was confirmed using SAED and AEM. The X-ray analyses were obtained with an EDAX energy-dispersive spectrometer and Princeton Gamma-Tech System IV analyzer. AEM procedures follow those described by Livi and Veblen (1987).

CHLORITOID MICROSTRUCTURES

Green Mountains samples

The subhedral chloritoid crystals from the Jamaica area contain abundant, narrow lamellae of chlorite and stilpnomelane. These sheet silicate lamellae occupy about 3% of the crystals, are typically ~8 to 20 nm wide, and are in crystallographic continuity with the chloritoid (Fig. 2). Occasional larger lamellae of chlorite and a 1:1 layer silicate mineral compositionally consistent with berthierine

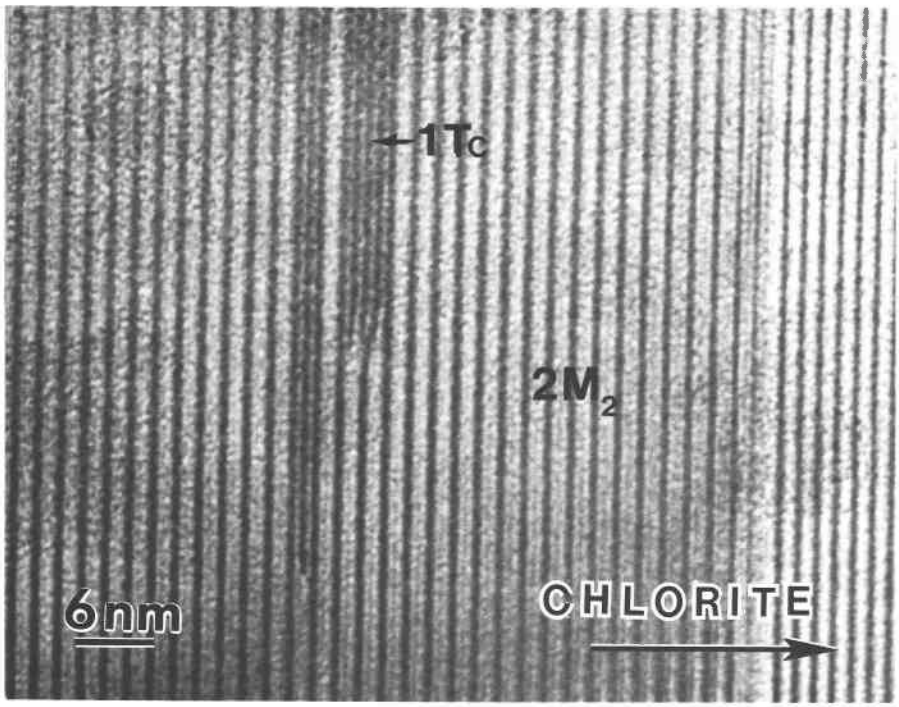

Fig. 4. HRTEM image of intergrown $2M_2$ and *1Tc* chloritoid polytypes. The apparently strain-free termination of a packet of *1Tc* in the $2M_2$ chloritoid is illustrated, and part of a chlorite lamella is shown at the right.

(up to 400 nm wide), as well as arrays of semirandomly oriented chlorite, paragonite, and muscovite crystals, have apparently developed in channels within chloritoid or formed at low-angle grain boundaries (Fig. 3). Electron-diffraction patterns from chlorite, stilpnomelane, and berthierine indicate that the lamellae possess varying degrees of stacking disorder.

Electron micrographs and SAED patterns from chloritoid reveal the presence of both the $2M_2$ and *1Tc* polytypes. Two-layer (monoclinic) chloritoid is generally the most abundant polytype in the specimens studied. Planar defects produced by variations in layer-stacking sequence are similar to those reported by Jefferson and Thomas (1978). Terminating stacking defects (Fig. 4), where packets of the *1Tc* polytype pass directly into the two-layer polytype, occur without observable strain contrast, resembling terminations associated with the $2M_1$ and $2M_2$ polytypes reported by Jefferson and Thomas (1978).

Chlorite lamellae. The narrow lamellae of sheet silicates in chloritoid occur in precise, crystallographically controlled orientations. Electron-diffraction patterns of intergrown chlorite and chloritoid (Fig. 5) show that *a* of chloritoid is parallel to *b* of chlorite, and *b* of chloritoid is parallel to *a* of chlorite. The c^* axes of chlorite and chloritoid, and hence their (001) planes, also are exactly parallel. Thus, the chloritoid/chlorite intergrowths can be described as topotactic.

Electron micrographs of narrow chlorite lamellae terminating in chloritoid suggest that intergrowth of these minerals occurs without appreciable strain of either structure; assuming that replacement occurred, it did so by conserving volume (Fig. 6). The interfaces illustrated in Figure 6 are generally sharp, and there are ledges in the (001) boundaries. This texture is similar to those observed in exsolution and replacement reactions involving chain silicates (Vander Sande and Kohlstedt, 1974; Champness and Lorimer, 1976; Veblen and Buseck, 1981). Although the direction of the reaction is not rigorously indicated, these observations suggest that replacement took place in part by the nucleation and propagation of ledges on the lamellar interfaces.

The possibility that some structural elements are inherited across non-(001) interfaces is suggested by the tightness of the interfaces and the continuity of some fringes across these boundaries in Figure 6. Indeed, both structures possess similar octahedral sheets, so that such a relationship also might be expected purely on structural grounds. Interfaces oriented at a low angle to (001) also show apparent structural continuity. Low-angle boundaries between chlorite and chloritoid, such as the boundary shown in Figure 7, similarly are tight, suggesting again that there may be some bonding between the two minerals across their interfaces, even when they are not perfectly oriented with respect to each other. These and other images of non-(001) interfaces typically show the narrow dark fringes of chlorite turning into either the white or black fringes of chloritoid. Under our imaging conditions, the narrow dark chlorite fringes correspond to the bruc-

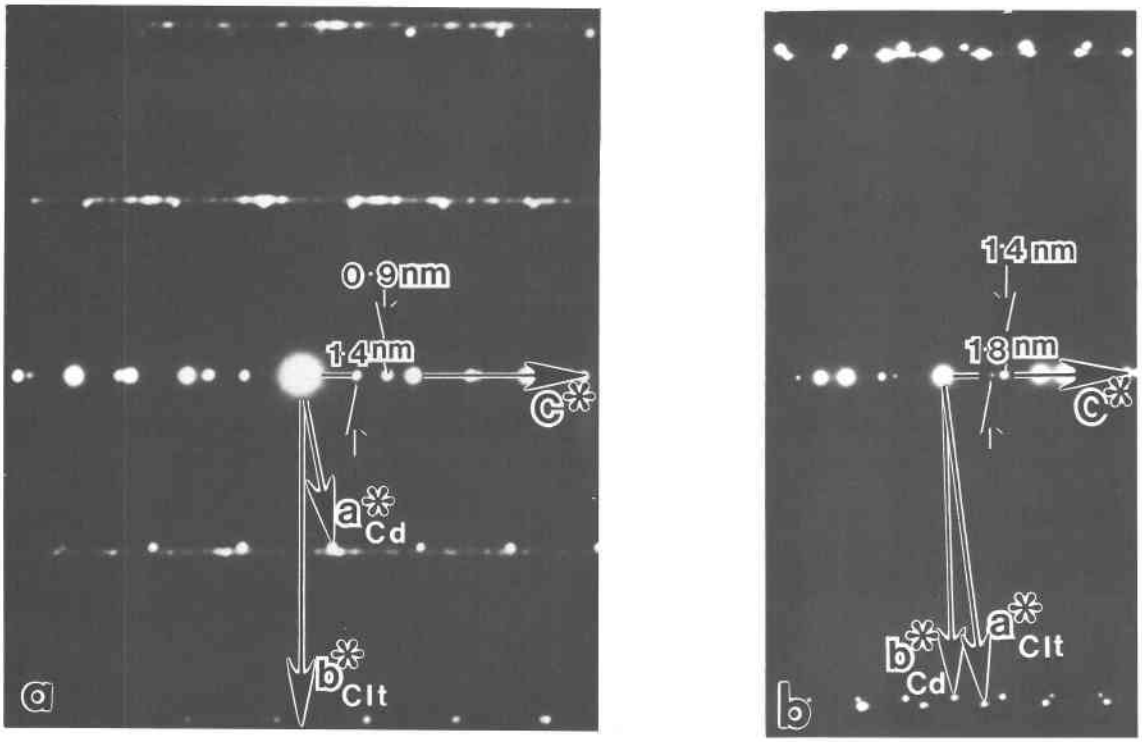

Fig. 5. Electron-diffraction patterns from an intergrowth of chlorite (1.4-nm basal spacing) and chloritoid (0.9-nm basal spacing). (a) *h*0*l* chloritoid and 0*kl* chlorite; (b) 0*kl* chloritoid and *h*0*l* chlorite.

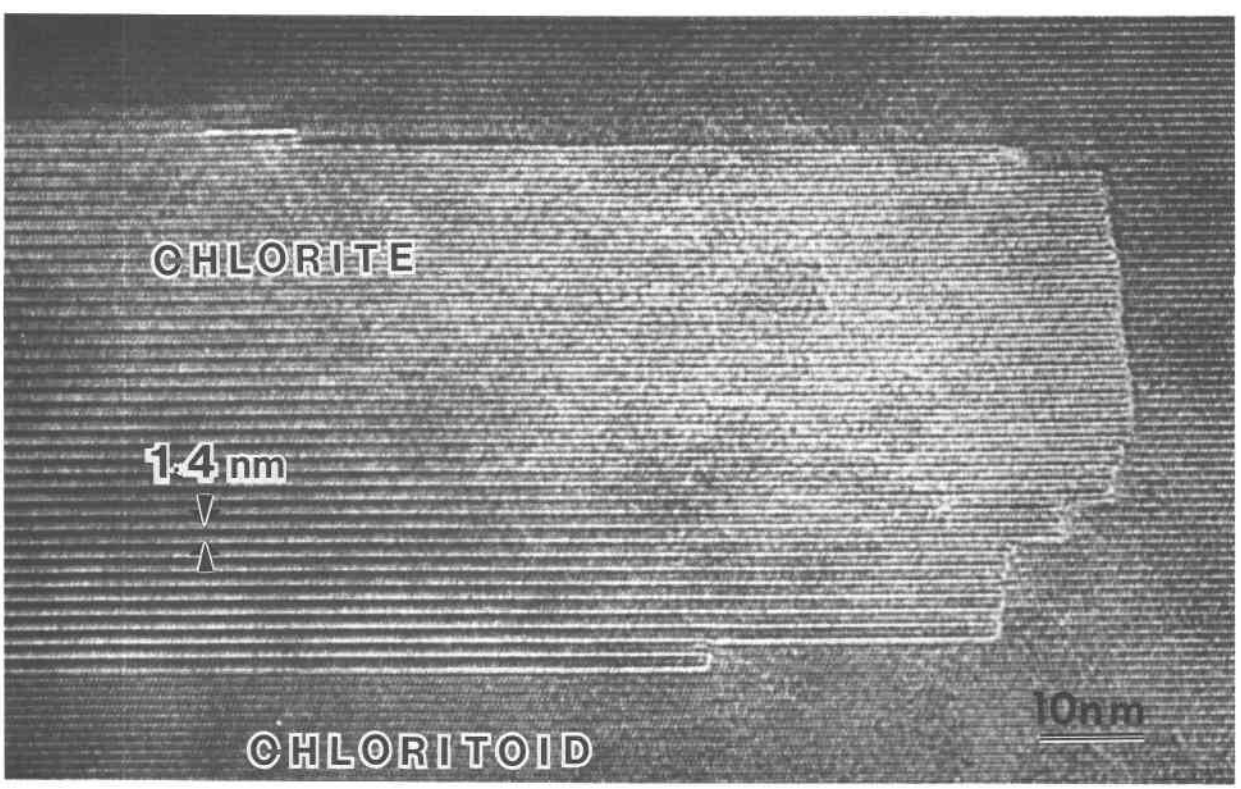

Fig. 6. A chlorite lamella terminating in chloritoid. There are no major gaps between the two structures, and there is apparent continuity of some lattice fringes across the boundary.

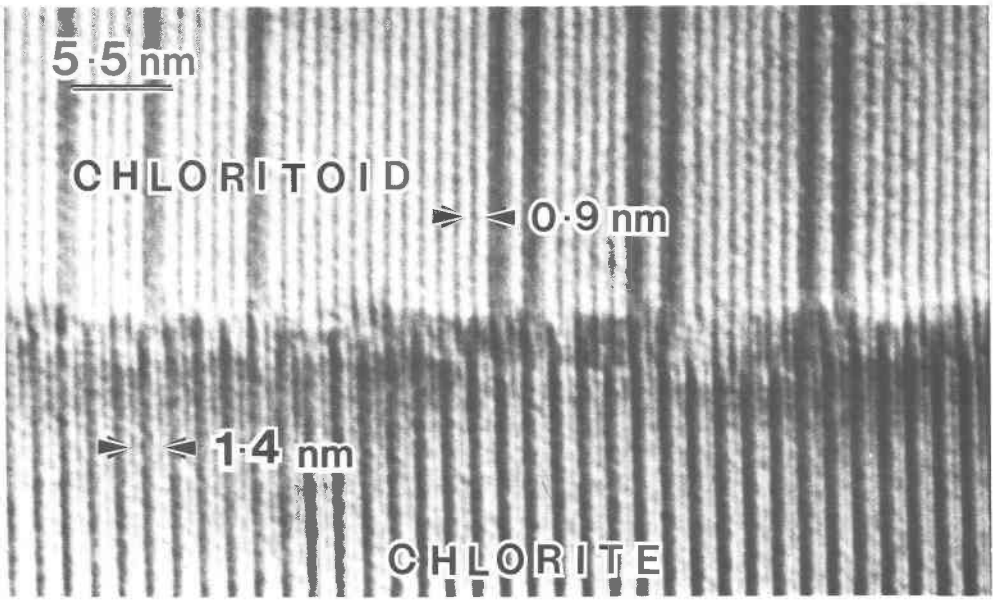

Fig. 7. Transmission electron micrograph of a low-angle grain boundary between chloritoid and chlorite; the interface is at approximately a right angle to the (001) planes. The 0.9-nm chloritoid fringes represent one-half of the monoclinic cell, and the dark, nonperiodic fringes are stacking faults. The continuity of some lattice fringes suggests that there may be bonding across the interface.

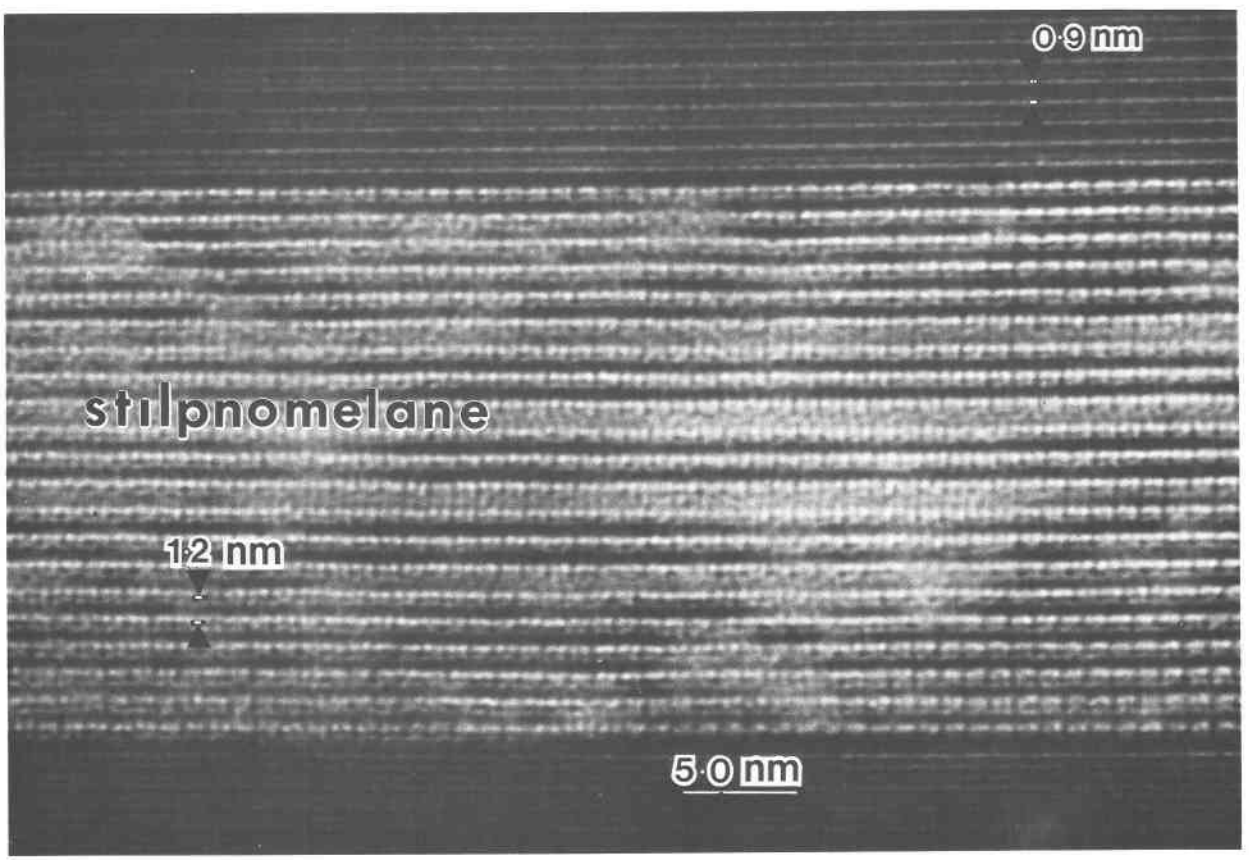

Fig. 8. The widest stilpnomelane lamella observed in chloritoid. Considerable stacking disorder is apparent in the stilpnomelane and can best be seen by sighting along the crooked cross-fringes approximately normal to the layers.

TABLE 1. Average structural formulae from AEM analyses of intergrown chloritoid and chlorite, Jamaica, Vermont

	Chloritoid	Chlorite
Si	1.99	2.44
Al	4.01	3.56
Mg	0.37	2.12
Fe*	1.61	1.65
Mn	0.03	0.01
Na	0.00	0.00
K	0.00	0.00
Ca	0.00	0.00
O**	10.00	10.00
OH**	2.00	8.00
Σ_{cation}	8.01	9.78

* All Fe calculated as Fe^{2+}.
** O and OH by stoichiometry.

ite-like sheets (Spinnler et al., 1984), and the centers of both the white and black fringes in chloritoid are at the positions of the two different octahedral sheets (App. 1). The HRTEM data thus suggest that either of the two octahedral sheets of chlorite can be continuous with either sheet of chloritoid.

Average AEM analyses of the chloritoid and chlorite are given in Table 1. We attempted to obtain analyses of the chloritoid with a fine spot (~10-nm beam diameter) to determine whether interpretable zoning patterns, such as solute depletion adjacent to chlorite lamellae, could be detected. All of the variation in chloritoid composition with distance from the lamellae was within the uncertainty associated with the analytical technique.

Stilpnomelane lamellae. In addition to chlorite, narrow lamellae of stilpnomelane were identified within the chloritoid by SAED patterns and their periodicities in HRTEM images. Most of these lamellae are three or four unit cells wide, but they range up to a maximum of 20 unit cells. Approximately 10% of the narrow lamellae observed in the Green Mountains chloritoids are composed at least in part of this mineral.

Streaking of stilpnomelane reflections parallel to c^* in electron-diffraction patterns from some lamellae is greater than that expected from the shape effect for thin crystals. This streaking suggests that the stilpnomelane possesses considerable stacking disorder. The variable orientation of cross-fringes in the HRTEM image of the widest observed stilpnomelane lamella (Fig. 8) confirms the irregular stacking sequence. Like the chlorite, stilpnomelane lamellae can terminate in chloritoid. Figure 9 shows such a feature, with some strain contrast associated with the termination. Continuity of lattice fringes between chloritoid and stilpnomelane may be indicated in this image.

Electron-diffraction patterns from more-ordered lamellae (Fig. 10) show that, like the chlorite, stilpnomelane tends to grow in an orientation crystallographically related to that of the host chloritoid. The *b*-axis electron-diffraction patterns from the intergrown minerals indicate that c^* axes of stilpnomelane and chloritoid are parallel,

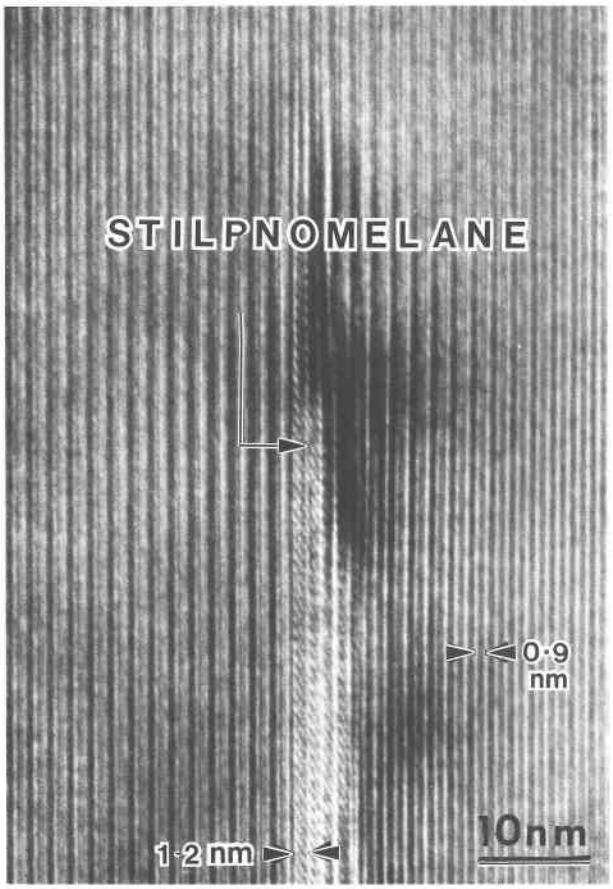

Fig. 9. HRTEM image showing strain contrast associated with the termination of a stilpnomelane lamella in chloritoid.

whereas a^* of stilpnomelane is inclined to a^* of chloritoid, representing a 30° angle between the *a* axes of these minerals (Fig. 10a). Figure 10b shows that $[31\bar{1}]^*$ of chloritoid is almost exactly parallel to $[11\bar{1}]^*$ of stilpnomelane. In real space, this indicates that the $(31\bar{1})_{cd}$ and $(11\bar{1})_{stp}$ planes are parallel, and the $[110]_{cd}$ and $[110]_{stp}$ directions are nearly parallel.

Berthierine lamellae. A sheet silicate with a 0.7-nm basal spacing is also present within the chloritoid (Fig. 11a); 1.4-nm 001 spots are not present in the SAED patterns, showing clearly that the mineral is not a chlorite. The Fe-rich, highly aluminous composition and diffraction patterns are consistent with berthierine, as defined by Bailey (1980). The berthierine forms lamellae of varying thickness that appear to penetrate into the chloritoid structure. Some slightly wider layer spacings are also observed (Fig. 11b; see arrows). These measure about 0.9 nm and possibly represent individual layers of mica (e.g., paragonite) or talc intergrown with the berthierine. Like stilpnomelane and chlorite, the berthierine lamellae are oriented crystallographically with respect to the host chloritoid. The c^* directions of chloritoid and berthierine are parallel, and although the structural form of berthier-

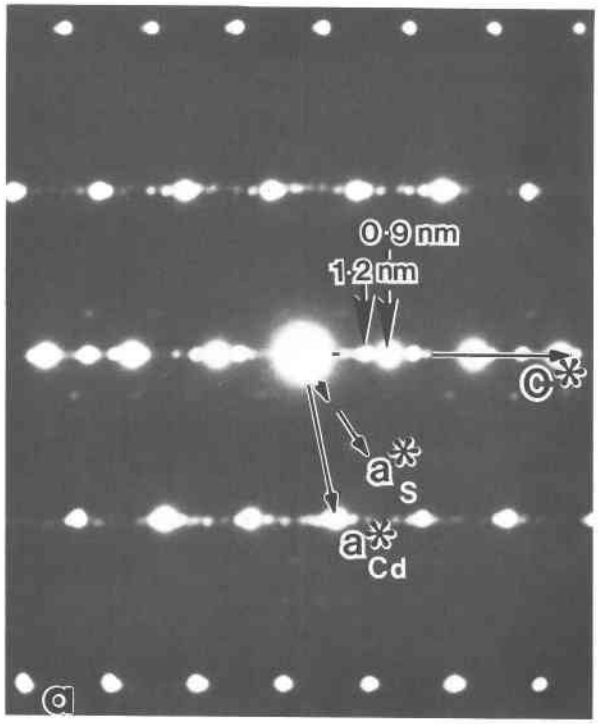

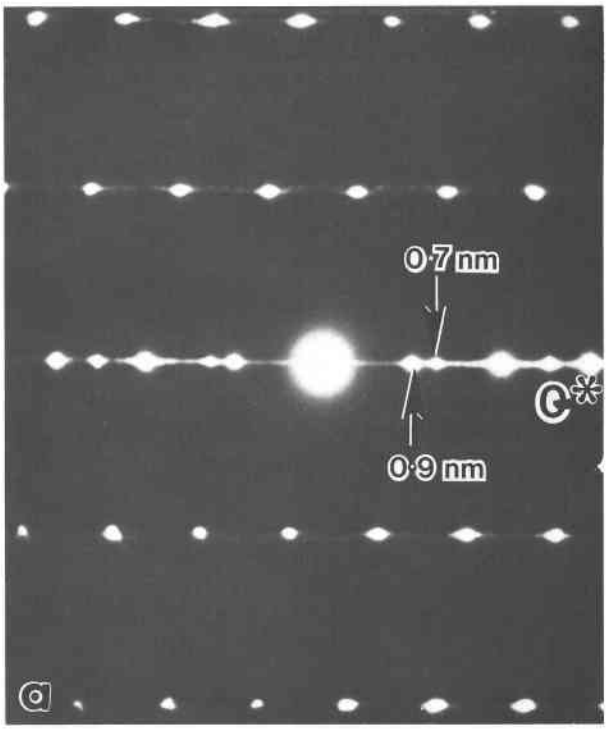

Fig. 11. (**a**) SAED pattern from berthierine (0.7-nm basal spacing) intergrown with chloritoid. (**b**) HRTEM image of stepped berthierine lamellae penetrating into chloritoid. Arrows indicate lattice spacings that are wider than normal in berthierine (approximately 1 nm, instead of 0.7 nm).

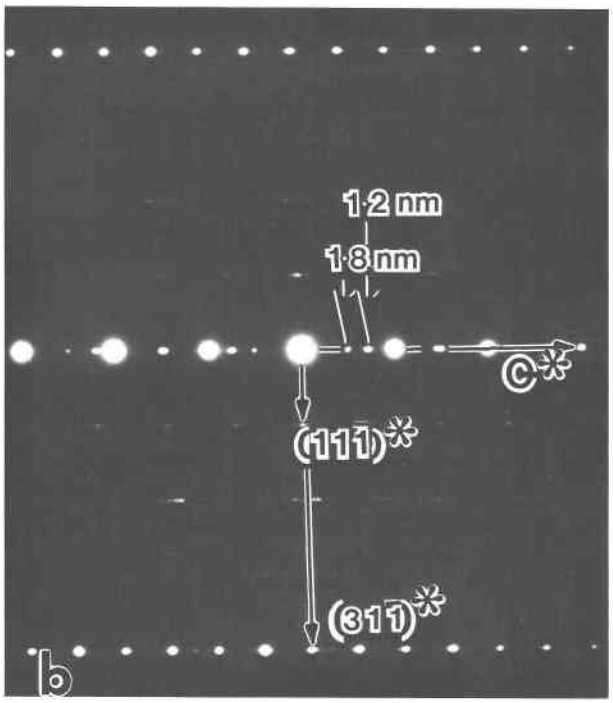

Fig. 10. SAED patterns from chloritoid-stilpnomelane intergrowths. (**a**) Pattern obtained with the electron beam parallel to *b* of both chloritoid and stilpnomelane. The *c** axes of the two minerals are parallel, and *a* of stilpnomelane is inclined 30° to that of chloritoid. (**b**) Pattern obtained with electron beam parallel to [1$\bar{1}$0] of stilpnomelane. The [110] directions of the two minerals are nearly parallel.

ine is uncertain, *a* chloritoid is probably parallel to *b* berthierine (and vice versa).

Other intergrown minerals. Paragonite and goethite also have been observed to form narrow, oriented lamellae parallel to (001) in chloritoid. Like the chlorite, stilpnomelane, and berthierine lamellae, these other minerals were identified with a combination of SAED, HRTEM, and AEM methods. Although they do occur alone, paragonite and goethite more commonly occur in hybrid lamellae with one or more other minerals, as discussed below.

Hybrid lamellae. Both stilpnomelane and chlorite coexist within some individual narrow lamellae in chloritoid. This is shown in Figure 12, where one layer passes directly from chlorite to stilpnomelane, apparently with some structural continuity and with only minor disruption or deflection of surrounding layers. This micrograph clearly illustrates the ease with which chloritoid, chlorite, and stilpnomelane can intergrow. Packets of a few mica layers with 0.95-nm layer widths also are locally intergrown with chlorite in some lamellae. Similar mica layers also form larger lamellae; their composition and basal spacing are consistent with paragonite (Figs. 13a, 13b). Goethite also forms most commonly as hybrid lamellae with berthierine (Fig. 14).

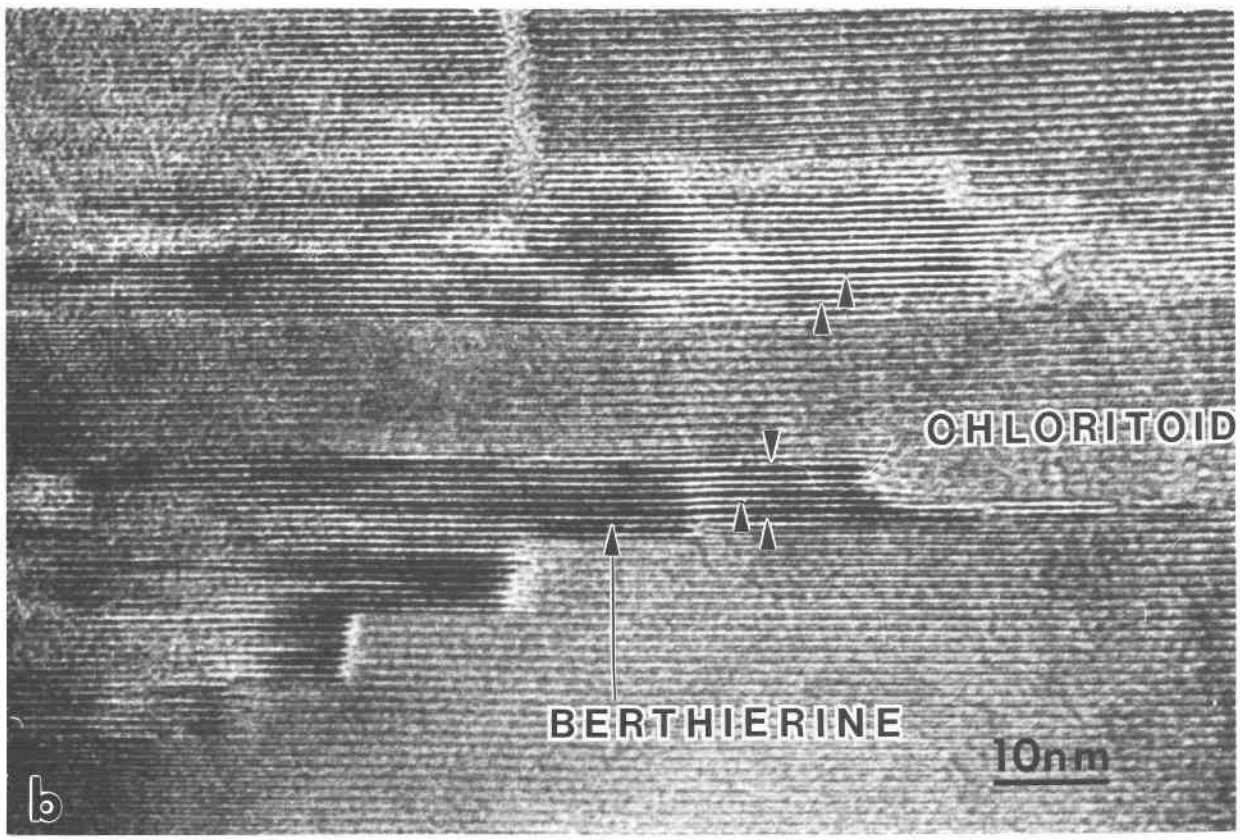

Fig. 11—Continued.

Taconic Range samples

AEM and electron diffraction were used to identify chloritoid in the Taconic samples. Although a small amount of chloritoid can be seen in these specimens with a petrographic microscope (see above), TEM observations indicate that most of the chloritoid in these rocks is smaller than the resolution of a light microscope (crystals typically are 20 to 50 nm in longest dimension). These minute crystals of chloritoid commonly are enclosed by or adjacent to chlorite, paragonite, or muscovite.

SAED patterns indicate that the chloritoid is predominantly a two-layer polytype with some stacking disorder. It is not rigorously crystallographically oriented with respect to the surrounding sheet silicates. Furthermore, TEM observations (Fig. 15) show that these small crystals are devoid of inclusions and lack sheet-silicate lamellae such as those in the Green Mountains chloritoid. These textures suggest that the growth of chloritoid in the Taconic phyllites did not occur by topotactic replacement of chlorite or another sheet silicate by chloritoid; such a mechanism would produce oriented intergrowths and would probably leave areas of sheet silicate in the chloritoid. Instead, it appears that chloritoid formed by unoriented nucleation and growth, without direct inheritance of any structural elements from the minerals of the lower-grade assemblage.

Discussion

Origin of chloritoid-sheet silicate intergrowths

As noted above, previous studies of the Jamaica region indicate that the Green Mountains samples experienced a complex polymetamorphic history (Karabinos, 1981, 1984). It is thus likely that the assemblage of chloritoid, chlorite, paragonite, stilpnomelane, and berthierine resulted from a combination of prograde and retrograde events. Although it can be difficult to determine the origin of sheet-silicate intergrowths using textural evidence alone, it is clear in these samples that retrograde chlorite partially replaced garnet, and it is also likely that relatively large, semirandomly oriented chlorite laths found in fractures in chloritoid (e.g., Fig. 3) represent the retrograde replacement of chloritoid. On the other hand, the narrow lamellae of chlorite in chloritoid conceivably could result from several processes: (1) prograde, topotactic replacement of chlorite by chloritoid, which left relict lamellae of the pre-existing chlorite (first prograde event: Fig. 1); (2) simultaneous parallel nucleation and growth of both chloritoid and chlorite; (3) topotactic growth of chlorite

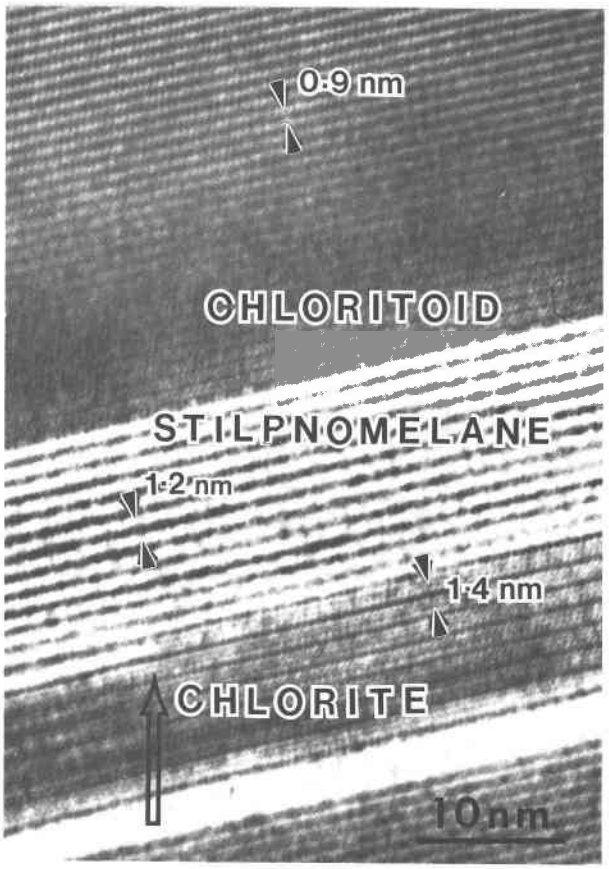

Fig. 12. A hybrid lamella in chloritoid containing both stilpnomelane and chlorite. The area indicated by the arrow shows a unit cell of stilpnomelane passing directly into a unit cell of chlorite.

as a result of the staurolite-forming reaction (Fig. 1) during the second prograde event; or (4) topotactic growth of chlorite lamellae in chloritoid during the strong retrograde metamorphic event.

Several reactions involving replacement of chlorite, as in possibility 1, have been suggested previously as mechanisms for chloritoid formation in metapelites (e.g., Thompson and Norton, 1968; Miyashiro, 1973, p. 205). However, the rigorous orientation relationship between chloritoid and sheet-silicate lamellae implies that such a reaction would have to be topotactic, and we have seen that chloritoid growth in the Taconic Range samples is not a topotactic reaction. We believe that application of results from the low-grade, regionally metamorphosed and deformed, Al-rich metapelites of the Taconic Range to the higher grade, regionally metamorphosed and deformed, Al-rich metapelites of the Green Mountains is valid, although we cannot demonstrate that all aspects of their metamorphic history were comparable (e.g., details of fluid flow).

Large chlorite crystals in the matrix of the Green Mountains samples have Fe-rich compositions and textures consistent with the interpretation that they formed during the first prograde greenschist-facies metamorphic event. These crystals show no indication of partial replacement by chloritoid. If chloritoid were topotactically replacing chlorite, it is not clear why some crystals would have been almost entirely replaced, while other, adjacent crystals were left completely unreacted. Consequently, we suggest that the dissolution-reprecipitation mechanism observed at the chloritoid isograd was also responsible for the crystallization of chloritoid in the Green Mountains samples (hence, relict, topotactically oriented chlorite lamellae should not be observed within chloritoid). We also note that the chloritoid contains narrow lamellae of several minerals other than chlorite, which would not have been produced by simple replacement of homogeneous chlorite by chloritoid. These textures are more consistent with the formation of narrow nuclei of chlorite and other minerals within chloritoid than they are with direct replacement of chlorite by chloritoid.

The second possibility, that the intergrowths result from simultaneous, oriented growth of chloritoid and sheet silicates, seems unlikely for many of the same reasons. Furthermore, the reaction sequence outlined in Figure 1 indicates that chloritoid and chlorite are only produced simultaneously as a consequence of destruction of garnet (and these reaction products are intimately associated with the garnet).

The third possibility, that chlorite formed because of breakdown of chloritoid during the second prograde event, is rejected on the basis that the chlorite lamellae are found within chloritoid in samples where the necessary staurolite-forming reaction did not occur.

The fourth possibility, that the sheet-silicate lamellae formed by replacement of chloritoid during retrograde metamorphism, is consistent with the petrological history of these rocks and with the observed textures. The Green Mountains samples experienced intense retrograde metamorphism. Indeed, the chlorite-chloritoid intergrowths are best developed in samples in which the effects of the intermediate retrogression, described by Karabinos (1984), are greatest and those of the second prograde metamorphism are least developed. Furthermore, replacement reactions in layer minerals commonly result in very narrow lamellae of the reaction products that occasionally terminate in the host, similar to the texture observed here (Veblen and Ferry, 1983; Eggleton and Banfield, 1985; Banfield and Eggleton, 1988; Maresch et al., 1985; Olives Baños and Amouric, 1984).

Although we cannot unequivocally discern between the two most probable origins for the chlorite lamellae (the first prograde versus the retrograde event: see asterisks in Fig. 1), we argue that the evidence strongly favors the interpretation that the narrow sheet-silicate lamellae in the Green Mountains chloritoids resulted from topotactic replacement during retrograde metamorphism. Furthermore, we suggest that a lamellar intergrowth microstructure is the predictable result of retrograde metamorphism that proceeds without simultaneous strong deformation.

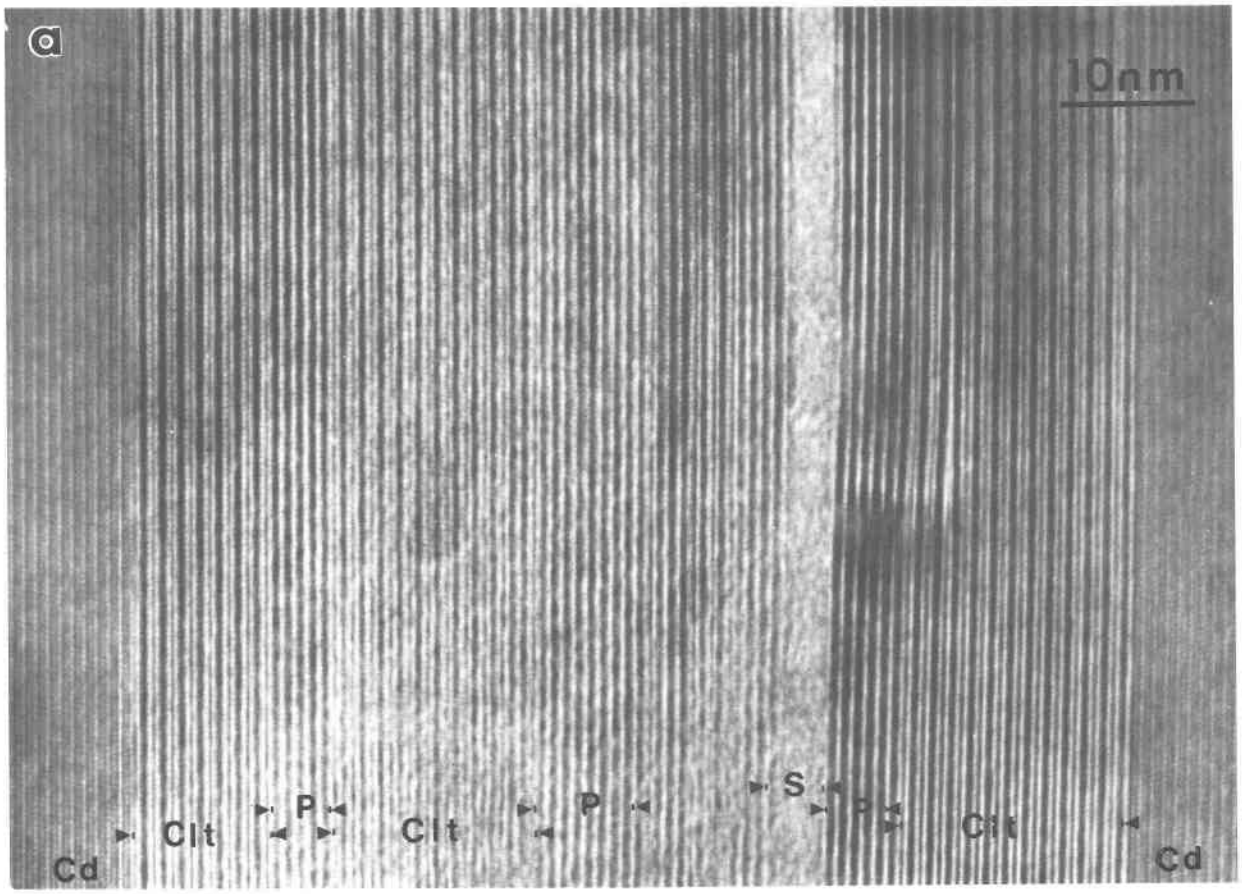

Nucleation of widely spaced lamellae is characteristic of a reaction that is controlled by diffusion (Fisher, 1978), a factor that is unlikely to limit reactions that occur during dynamic, prograde metamorphism.

Chemistry of the chloritoid–sheet-silicate reactions

In occurrences where sheet-silicate intergrowths have resulted from replacement, a reaction can be written based on the chemistry of the reactant and product minerals and the structural reaction mechanism as deduced from HRTEM observations (as in replacement reactions involving biotite and chlorite: Veblen and Ferry, 1983; Eggleton and Banfield, 1985; Maresch et al., 1985). In effect, the HRTEM observations allow the volume change associated with the reaction to be estimated, which gives the ratio of the reaction coefficients for the reactant and product

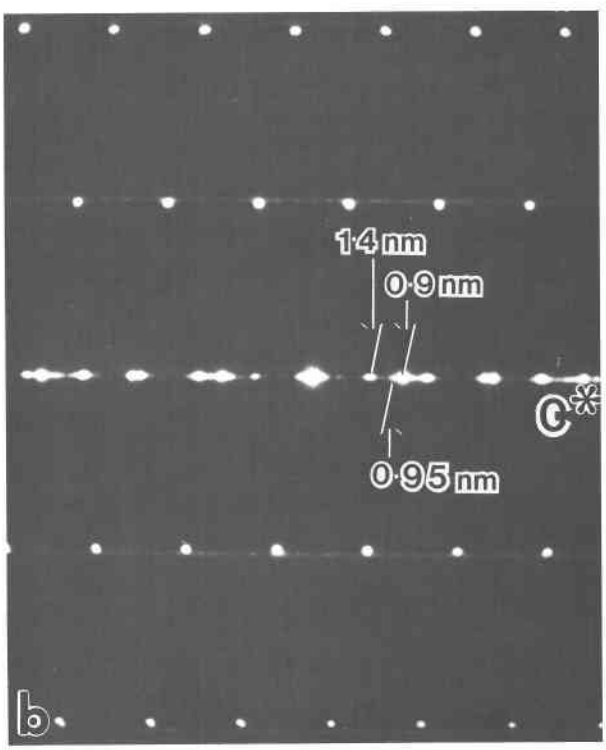

→

Fig. 13. (**a**) A hybrid lamella in chloritoid (Cd) containing chlorite (Clt), paragonite (P), and beam-damaged stilpnomelane (S). (**b**) SAED pattern from this hybrid lamella illustrating the 0.95-nm basal spacing associated with paragonite, 1.4-nm repeat of chlorite, and 0.9-nm spacing from the surrounding chloritoid.

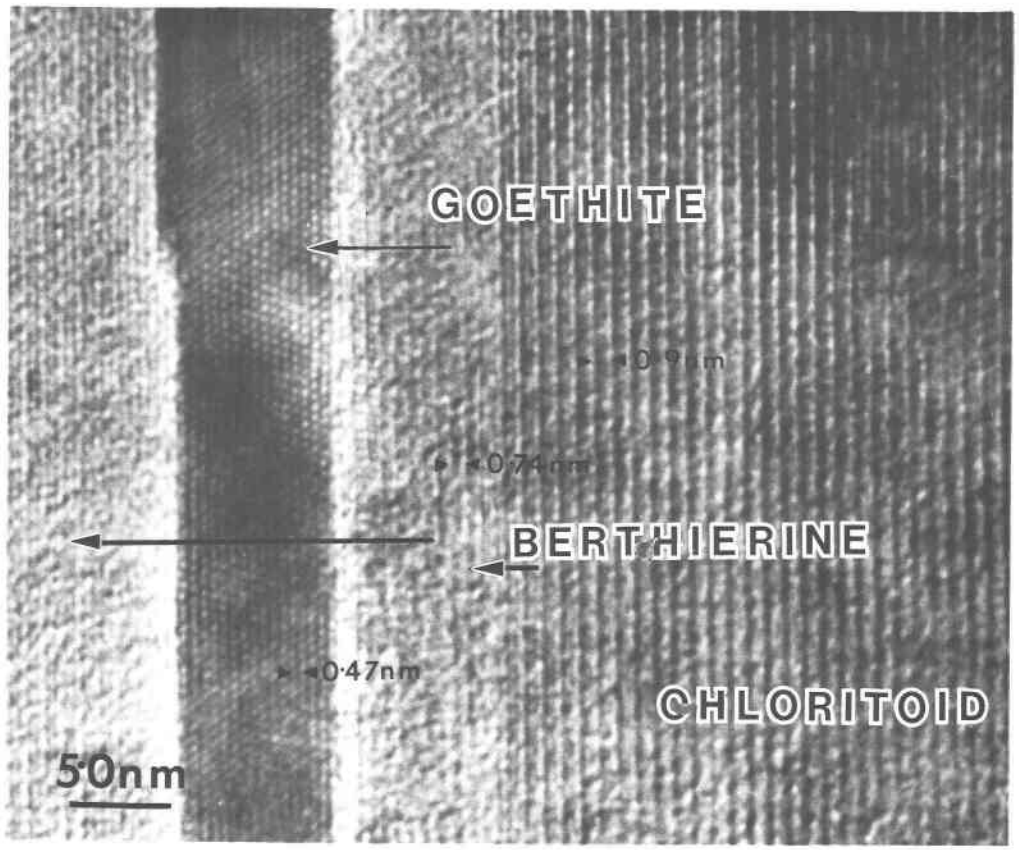

Fig. 14. A hybrid lamella of berthierine and goethite in chloritoid.

minerals. It has been observed in these studies that the chemistry of the daughter mineral and that of the parent can be closely related, with the bulk of the material for the product mineral being inherited from the parent and only some components necessarily being added or subtracted, presumably via a fluid phase.

In the Green Mountains chloritoids, HRTEM images indicate that chlorite formed narrow lamellae in chloritoid, rather than producing a finely interstratified, mixed-layer chlorite-chloritoid material. Assuming that the textural and geologic interpretation in the last section is correct, the lack of substantial strain at lamellar tips in TEM images indicates that chlorite replaced approximately an equal volume of chloritoid. In the present case, an equal-volume transformation implies that almost exactly $\frac{4}{3}$ unit cells of one-layer chlorite replaced each unit cell of monoclinic (two-layer) chloritoid. (The chlorite coefficient is $\frac{4}{3}$ within the error of the ratio of unit-cell volumes from our electron-diffraction patterns. In addition, the chlorite unit-cell volume calculated with the regression equations of Hey, 1954, is 0.693 nm^3, so that $\frac{4}{3} \cdot V_{chl} = 0.924$ nm^3; this compares with the choritoid unit-cell volume from Hanscom, 1975, of 0.925 nm^3.)

TABLE 2. Chemical balance for equal-volume reaction of chloritoid to chlorite*

	1 chloritoid	$\frac{2}{3}$ chlorite	Fluid**
Si	1.99	1.62	0.37
Al	4.01	2.37	1.64
Mg	0.37	1.41	−1.04
Fe	1.61	1.10	0.51
Mn	0.03	0.01	0.02
O	12.00	12.00	0.00
H	2.00	5.33	−3.33

* Assumes that no changes in composition of the chloritoid or chlorite have occurred since replacement; see text.

** Negative numbers indicate that the component is consumed by the reaction, i.e., is removed from the fluid.

The coefficients for an equal-volume reaction of chloritoid to chlorite are given in Table 2 (the chlorite coefficient of $\frac{2}{3}$ results from the fact that Z = 4 and 2 for monoclinic chloritoid and one-layer chlorite respectively, for the formula units used in Table 1). Table 2 suggests that some exchange with metamorphic fluids is necessary for all major chemical components, in order for the reaction to proceed. Substantial amounts of H and Mg must enter the reaction site and be removed from the metamorphic fluid, whereas Si, Al, and Fe would be given up to the fluid.

The reaction in Table 2 assumes that the chloritoid being replaced had the typical composition given in Table 1 since the onset of reaction. However, the narrow la-

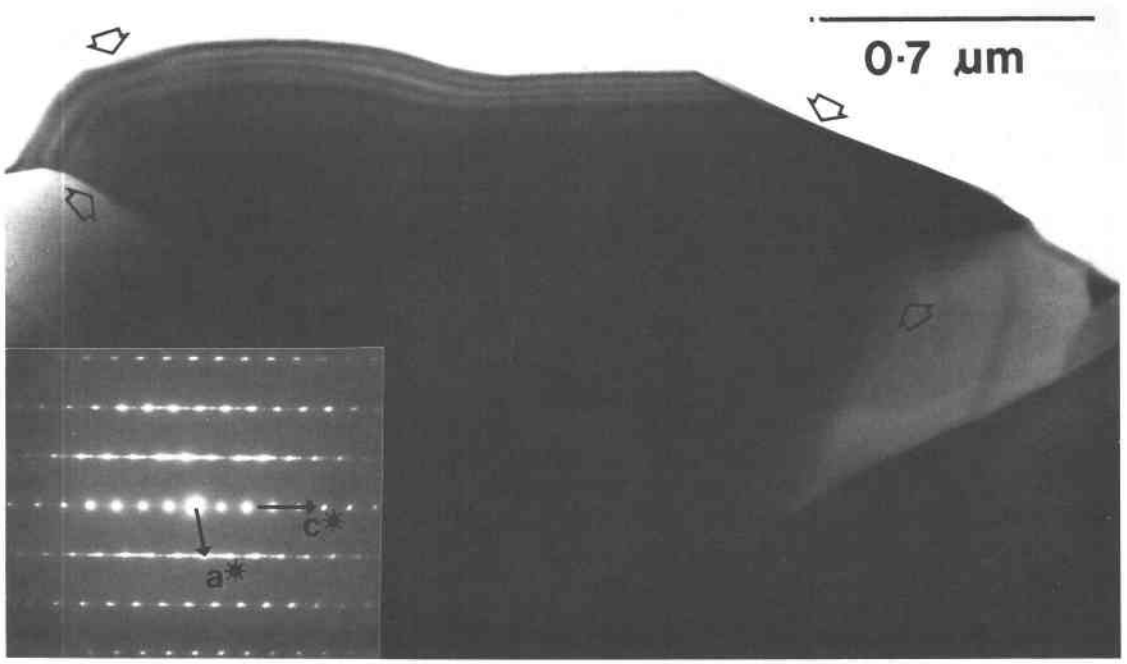

Fig. 15. A small, randomly oriented chloritoid crystal formed by simple prograde reaction in a metapelite from the Taconic Range. The chloritoid does not contain lamellae of a precursor mineral, although the inset SAED pattern and other images indicate that it possesses stacking disorder. Arrows indicate the extent of the chloritoid crystal.

mellae of chloritoid and chlorite have experienced a protracted regional metamorphic history, so that it may be expected that they will have re-equilibrated following replacement. The Fe/Mg in the chloritoid and chlorite appear to preserve compositions indicating equilibration between garnet and staurolite (based on the calibration of Ashworth and Evirgen, 1984), appropriate for either the early stage of the retrograde event, or reflecting compositional re-equilibration during the second prograde event. The minerals may also have changed composition during the reaction. Consequently Table 2 probably does not accurately represent the precise chemical exchanges occurring at the time of replacement, but reflects the effect of the initial structural replacement process, plus any subsequent exchange reactions, involving for example, $FeMg_{-1}$ and $FeAl_{-1}$.

It is possible that much of the chemical exchange required to form the chlorite occurred between the lamellae and the remaining chloritoid, rather than with the metamorphic fluid. Only about 3% by volume of the chloritoid (average Mg/[Fe + Mg] $\simeq$ 0.187) is occupied by chlorite. The initial Mg/[Fe + Mg] of the chloritoid need be only about 0.201 for all the Mg required to form the chlorite to have been derived from chloritoid, and all the Fe released to have been absorbed by chloritoid by continuous reaction. Indeed, the formation of the chlorite lamellae might be a response to the decreasing stability of Mg-rich chloritoid with decreasing temperature. Although it seems likely that the reaction proceeded by exchange of Si, Al, Mg, Fe, and H with both fluid and host chloritoid, it is not possible to determine the exact sources and sinks for the reaction. In addition, the presence of other sheet-silicate lamellae, such as stilpnomelane and berthierine, suggests that an accurate description of the reactions would have to include these solid phases, as well as the chlorite and chloritoid. These other minerals may well have acted as sinks for Si, Al, and Fe produced by the chloritoid-chlorite reaction.

As noted in the last section, it is likely that stilpnomelane lamellae, like those of chlorite, formed during retrograde metamorphism. In any case, the fact that stilpnomelane commonly forms hybrid lamellae with chlorite suggests that the origin of the two minerals is closely related. Stilpnomelane is relatively poor in Al, and its development in intimate intergrowths with chlorite and chloritoid is rather surprising. Chloritoid and stilpnomelane typically are self-exclusive in low-grade metapelites (e.g., Zen, 1960). Although a small three-phase field may exist far to the Fe-rich side of an AFM diagram at low grade, the interpretation of stilpnomelane + chloritoid + chlorite as an equilibrium assemblage would imply equilibration within the chloritoid crystal (not with the whole-rock bulk composition), and a chlorite composition far more Fe-rich than that observed for these lamellae. It is possible that stilpnomelane lamellae grew metastably, or during a separate metamorphic event by reaction of chloritoid or chlorite with Al-poor fluids. Although it is not possible to pinpoint the process that led to growth of stilpnomelane, this occurrence shows that the assemblage chloritoid + chlorite + stilpnomelane is

attainable and demonstrates that stilpnomelane can crystallize in rather aluminous environments.

It is possible that the other types of lamellae in the Green Mountains chloritoids, such as paragonite, berthierine, and goethite, also formed during the same retrograde event in which chlorite formed. However, these other minerals could well have formed at some other stage in the history of these intergrowths. Since chlorite is by far the most abundant mineral intergrown in the chloritoid, we have not considered the detailed chemistry of the reactions that produced these other lamellae.

Crystallographic controls on the intergrowths

The ability of chlorite, chloritoid, stilpnomelane, paragonite, and berthierine to form fine-scale, crystallographically controlled intergrowths is attributed to (1) the similarity of lattice periodicities normal to c^* in all these structures and (2) the fact that they all possess two-dimensionally infinite sheets of octahedrally coordinated cations (and, of course, tetrahedral units that can be articulated to these sheets). On structural grounds, it is likely that the lamellar interfaces consist of octahedral sheets that are shared by two different structures.

Measurement of numerous SAED patterns shows that interlayering occurs predominantly with a of chlorite parallel to b of chloritoid, and vice versa. However, two other orientations in which the a and b axes of chloritoid are inclined to those of chlorite by $\pm 60°$ were also observed (because of pseudohexagonal symmetry in the a-b plane). Since the fits between the dimensions of chloritoid and chlorite are similar in all three orientations, it is not surprising that the alternate arrangements were observed occasionally.

The linear misfit between a of chloritoid and b of chlorite is approximately 3%, and that between b of chloritoid and a of chlorite is about 2%. To apply this comparison to chloritoid and chlorite at elevated temperatures and pressures, it is necessary to assume that these minerals have similar thermal expansivities and compressibilities, or that the amount of change in unit-cell parameters is small compared to the misfits. In the present case, it appears that the relative changes in a and b dimensions are, in fact, negligible compared to the misfits, based on the temperature and pressure conditions for the Jamaica rocks (Karabinos, 1981) and on thermal-expansion data for chlorite and chloritoid and the compressibilities typical for sheet silicates (Symmes, 1986; Ivaldi et al., 1988; Hazen and Finger, 1978). The detailed mechanism by which the misfit is accommodated is not completely understood.

Electron-diffraction patterns indicate that the lattices of intergrown chloritoid and stilpnomelane fit together exactly in the (001) plane, within the resolution of the SAED technique. The zone illustrated in Figure 10a contains a^* and c^* of both minerals, indicating that the stilpnomelane and chloritoid b axes coincide (b of stilpnomelane is four times that of chloritoid). As in the case of the chloritoid-chlorite intergrowths, the chloritoid-stilpnomelane intergrowths can be described as topotactic.

Conclusions

We have used high-resolution and analytical transmission electron microscopy to show that chloritoid crystals in garnet-grade schists from Jamaica, Vermont, contain complex mixtures of intergrown sheet silicates. These sheet silicates form very narrow lamellae in orientations that are precisely controlled by the structure of the host chloritoid. In contrast, chloritoid that formed by simple prograde reactions in phyllites from the Taconic Range, Vermont, developed in random orientations relative to the sheet silicates in the matrix. This chloritoid contains no relict lamellae of precursor minerals. A variety of textural, chemical, and geologic evidence suggests that the intergrowths from Jamaica result from retrograde replacement of chloritoid by the sheet silicates.

The apparent ease with which chloritoid, chlorite, stilpnomelane, paragonite, and berthierine can intergrow on (001) is attributed to similarities in lattice spacings parallel to their sheets of octahedra. Continuity of lattice fringes between chloritoid-chlorite, chloritoid-stilpnomelane, and chlorite-stilpnomelane may indicate that reactions between these minerals involve partial inheritance of octahedral sheets. Intergrowth of all minerals in the Jamaica samples occurred without the development of regular gaps or significant disruption of the structures, indicating the isovolumetric nature of the reactions.

Although the crystallography of the intergrowths is relatively straightforward, the detailed chemistry of the reactions that produced the intergrown sheet silicates is not easy to assess. It is possible that chloritoid re-equilibrated to more Fe-rich compositions stable at lower temperatures by the formation of chlorite lamellae that are relatively rich in Mg. However, the detailed chemical budgets between chloritoid, the various sheet silicates, and metamorphic fluids cannot be calculated with any certainty. It is likely that observed compositions have been altered by exchange reactions during subsequent prograde and retrograde metamorphism.

Acknowledgments

This paper benefited from discussions with John M. Ferry, Robert F. Martin, George W. Fisher, E-an Zen, Kenneth J. T. Livi, and Eugene S. Ilton. Helpful reviews were provided by Adrian Brearley and Laurel Goodwin. The research was supported by NSF grant EAR8609277. Jo Laird is thanked for editorial handling. Electron microscopy was performed at the Johns Hopkins high-resolution TEM lab, which was established with partial support from NSF instrumentation grant EAR8300365.

References cited

Ahn, J.H., and Peacor, D.R. (1986) Transmission and analytical electron microscopy of diagenetic chlorite in Gulf Coast argillaceous sediments. Clays and Clay Minerals, 34, 165–179.

Amouric, M., Mercuriot, G., and Barronet, A. (1981) On computed and observed HRTEM images of perfect mica polytypes. Bulletin de Minéralogie, 104, 298–313.

Ashworth, J.R., and Evirgen, M.M. (1984) Mineral chemistry of regional

chloritoid assemblages in the chlorite zone, Lycian nappes, south-west Turkey. Mineralogical Magazine, 48, 159–165.
Bailey, S.W. (1980) Structures of layer silicates. In G.W. Brindley and G. Brown, Eds., Crystal structures of clay minerals and their X-ray identification, p. 1–124. Mineralogical Society, London.
Banfield, J.F., and Eggleton, R.A. (1988) A transmission electron microscope study of biotite weathering. Clays and Clay Minerals, 36, 47–60.
Champness, P.E., and Lorimer, G.W. (1976) Exsolution in silicates. In H.-R. Wenk, Ed., Electron microscopy in mineralogy, p. 174–204. Springer-Verlag, Berlin.
Cowley, J.M., and Moodie, A.F. (1957) The scattering of electrons by atoms and crystals, I. A new theoretical approach. Acta Crystallographica, 10, 609–619.
Eggleton, R.A., and Banfield, J.F. (1985) The alteration of granitic biotite to chlorite. American Mineralogist, 70, 902–910.
Fisher, G.W. (1978) Rate laws in metamorphism. Geochimica et Cosmochimica Acta, 42, 1035–1050.
Halferdahl, L.B. (1961) Chloritoid: Its composition, stability, and occurrence. Journal of Petrology, 2, 49–135.
Hanscom, R.H. (1975) Refinement of the crystal structure of monoclinic chloritoid. Acta Crystallographica, B31, 780–784.
Hazen, R.M., and Finger, L.W. (1978) The crystal structures and compressibilities of layer minerals at high pressure. II. Phlogopite and chlorite. American Mineralogist, 63, 293–296.
Hey, M.H. (1954) A new review of the chlorites. Mineralogical Magazine, 30, 277.
Iijima, S., and Buseck, P.R. (1978) Experimental study of disordered mica structures by high-resolution electron microscopy. Acta Crystallographica, A34, 709–719.
Iijima, S., and Zhu, J. (1982) Electron microscopy of a muscovite-biotite interface. American Mineralogist, 67, 1195–1205.
Ivaldi, G., Catti, M., and Ferraris, G. (1988) Crystal structure at 25 and 700 °C of magnesiochloritoid from a high-pressure assemblage (Monte Rosa). American Mineralogist, 73, 358–364.
Jefferson, D.A., and Thomas, J.M. (1978) High resolution electron microscopic and X-ray studies of non-random disorder in an unusual layered silicate (chloritoid). Proceedings of the Royal Society of London, series A, 361, 399–411.
Karabinos, P. (1981) Deformation and metamorphism of Cambrian and Precambrian rocks on the east limb of the Green Mountains anticlinorium near Jamaica, Vermont. Ph.D. thesis, Johns Hopkins University, Baltimore, Maryland.
——— (1984) Deformation and metamorphism on the east side of the Green Mountain massif in southern Vermont. Geological Society of America Bulletin, 95, 584–593.
Karabinos, P., and Laird, J. (1988) Structure and metamorphism from Jamaica to the Athens dome, Vermont. In W.A. Bothner, Ed., Guidebook for field trips in southwestern Vermont, and north-central Massachusetts, p. 281–292. New England Intercollegiate Geological Conference, 80th Annual Meeting, 1988, Keene, New Hampshire.
Livi, K.J.T., and Veblen, D.R. (1987) "Eastonite" from Easton, Pennsylvania: A mixture of phlogopite and a new form of serpentine. American Mineralogist, 72, 113–125.
Maresch, W.V., Massonne, H.-J., and Czank, M. (1985) Ordered and disordered chlorite/biotite interstratifications as alteration products of chlorite. Neues Jahrbuch für Mineralogie Abhandlungen, 152, 79–100.
Miyashiro, A. (1973) Metamorphism and metamorphic belts, 492 p. Wiley, New York.
O'Keefe, M.A. (1984) Electron image simulation: A complementary processing technique. In Electron optical systems for microscopy, microanalysis, and microlithography, p. 209–220. Scanning Microscopy International, AMF O'Hare, Chicago.
Olives Baños, J., and Amouric, M. (1984) Biotite chloritization by interlayer brucitization as seen by HRTEM. American Mineralogist, 69, 869–871.
Ribbe, P.H. (1982) Chloritoid. Mineralogical Society of America Reviews in Mineralogy (2nd edition), 5, 155–170.
Rosenfeld, J.L. (1968) Garnet rotation due to major Paleozoic deformation in southeastern Vermont. In E. Zen, W.S. White, J.B. Hadley, and J.B. Thompson, Jr., Eds., Studies in Appalachian geology—Northern and maritime, p. 185–202. Wiley, New York.
Spear, F.S., and Cheney, J.T. (1989) A petrogenetic grid for pelitic schists in the system SiO_2-Al_2O_3-FeO-MgO-K_2O-H_2O. Contributions to Mineralogy and Petrology, 101, 149–164.
Spinnler, G.E., Self, P.G., Iijima, S., and Buseck, P.R. (1984) Stacking disorder in clinochlore chlorite. American Mineralogist, 69, 252–263.
Symmes, G.H. (1986) The thermal expansion of natural muscovite, paragonite, margarite, pyrophyllite, phlogopite, and two chlorites: The significance of high P/T volume studies on calculated phase equilibria. B.A. thesis, Amherst College, Amherst, Massachusetts.
Thompson, J.B., Jr., and Norton, S.A. (1968) Paleozoic regional metamorphism in New England and adjacent areas. In E. Zen, W.S. White, J.B. Hadley, and J.B. Thompson, Jr., Eds., Studies in Appalachian geology—Northern and maritime, p. 319–328. Wiley, New York.
Vander Sande, J.B., and Kohlstedt, D.L. (1974) A high resolution electron microscope study of exsolution in enstatite. Philosophical Magazine, 29, 1041–1049.
Veblen, D.R. (1983a) Exsolution and crystal chemistry of the sodium mica wonesite. American Mineralogist, 68, 554–565.
——— (1983b) Microstructures and mixed layering in intergrown wonesite, chlorite, talc, biotite, and kaolinite. American Mineralogist, 68, 566–580.
Veblen, D.R., and Buseck, P.R. (1981) Hydrous pyriboles and sheet silicates in pyroxenes and uralites: Intergrowth microstructures and reaction mechanisms. American Mineralogist, 66, 1107–1134.
Veblen, D.R., and Ferry, J.M. (1983) A TEM study of the biotite-chlorite reaction and comparison with petrologic observations. American Mineralogist, 68, 1160–1168.
Zen, E-an. (1960) Metamorphism of Lower Paleozoic rocks in the vicinity of the Taconic Range in west-central Vermont. American Mineralogist, 45, 129–175.
——— (1967) Time and space relationships of the Taconic allochthon and autochthon. Geological Society of America Special Paper 97, 107 p.

Manuscript received July 28, 1988
Manuscript accepted January 20, 1989

Appendix 1. Computer simulation of chloritoid HRTEM images

In order to interpret the experimental chloritoid HRTEM images rigorously, simulated images were computed using the SHRLI set of programs (O'Keefe, 1984), version 80F. These programs use the multislice method of Cowley and Moodie (1957) to calculate the effects of dynamical diffraction in the specimen, and the optics and operating parameters of the microscope are simulated. Refined atomic parameters for $2M_2$ chloritoid from Hanscom (1975) were used for the input structure. Images were calculated with the electron beam parallel to both the a and b axes for a range of microscope defocus values and specimen thicknesses ranging up to 14.2 nm. Microscope parameters for the simulations were appropriate for the Philips 420T at operating conditions used for this study, as follows: objective aperture radius = 4.37 nm^{-1}, semi-angle of convergence = 0.65 mrad, chromatic halfwidth = 15 nm, spherical aberration coefficient = 2.0 mm, vibration halfwidth = 0.05 nm.

The simulations show that for our imaging conditions, a-axis images consist of one-dimensional fringes, whereas imaging parallel to the b axis produces more complicated, two-dimensional images. This is consistent with our observations and with images published in the literature (e.g., Jefferson and Thomas, 1978). For images with one-dimensional fringes, such as many of those shown in this paper, there are only a few essentially different image types that occur for our experimental conditions, assuming that the specimen is in perfect orientation with respect to the electron beam; examples of these image types are shown in Appendix Figure 1. There is little variation in the basic image character with changes in specimen thickness up to our maximum

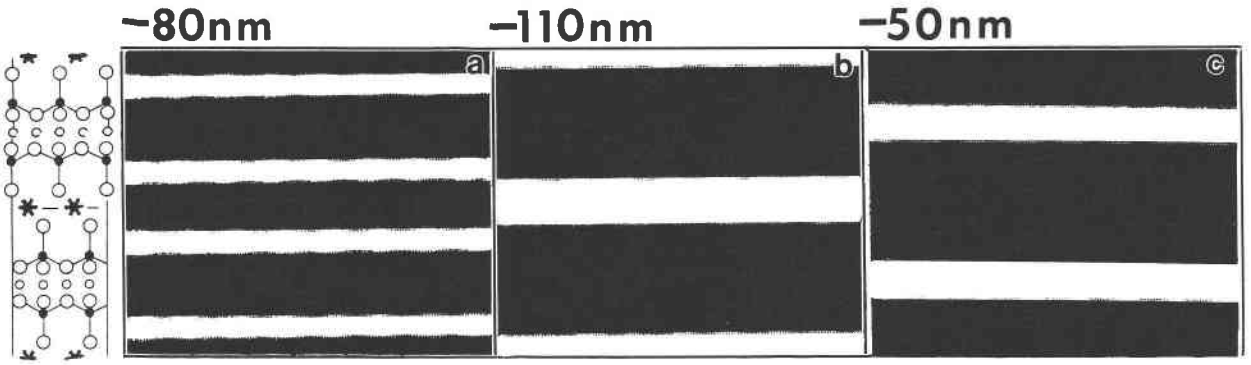

App. Fig. 1. Computer-simulated HRTEM images of monoclinic chloritoid obtained with the electron beam parallel to the *a* axis. Crystal thickness is 9.5 nm. (**a**) Defocus $\Delta f = -80$ nm. (**b**) $\Delta f = -110$ nm. (**c**) $\Delta f = -50$ nm. In schematic diagram to the left, rows of small circles indicate $(Al_3O_8)^{-7}$ and rows of asterisks indicate $[Fe_2^{2+}AlO_2(OH)_4]^{-1}$.

simulated thickness of 14.2 nm, and the calculated images shown in Appendix Figure 1 are all for a thickness of 9.5 nm.

For underfocus values around −80 nm, there are four dark and four light fringes per monoclinic unit cell, and the dark fringes are centered on every octahedral sheet (App. Fig. 1a). For more negative values of defocus starting at about −100 nm, there are only two dark fringes per unit cell (App. Fig. 1b); in this case, the dark fringes are centered on the relatively pure Al octahedral sheets (M2 sites), while the light fringes are centered on the relatively Fe-rich sheets (M1 sites). Similarly, for more positive values of defocus starting at about −60 nm, there also are only two dark fringes per cell, but in this case they overlie the Fe sheets (App. Fig. 1c). Since this contrast reversal takes place over a relatively narrow range of defocus, it is not possible to say whether the dark fringes correspond to the Al or the Fe-rich octahedral sheets, unless the microscopist has excellent control on his/her focus conditions. However, it is possible to state that the fringes do correspond to the positions of one of the octahedral sheets, and this is sufficient information to interpret the structural details of chloritoid-chlorite intergrowths, for example (see text).

For all one-dimensional chloritoid images that are obtained with the electron beam oriented perfectly parallel to the layers, the image periodicity is 0.9 nm, rather than the true 1.8-nm structural periodicity for two-layer, monoclinic chloritoid. Thus, information on the polytype of the chloritoid can only be obtained from two-dimensional, *b*-axis images or from one-dimensional images that have been recorded from crystals that are slightly out of orientation. Images exhibiting the polytypic periodicity, such as that shown in Figure 4, therefore cannot be interpreted reliably in terms of the detailed layers in the structure, but they are invaluable for elucidating the variations in stacking of the layers.